Hindawi Publishing Corporation
Advances in Physical Chemistry
Volume 2011, Article ID 407480, 6 pages
doi:10.1155/2011/407480

Research Article

$FeCr_2O_4$ Nanoparticles as Anode Catalyst for Ethane Proton Conducting Fuel Cell Reactors to Coproduce Ethylene and Electricity

Jian-Hui Li, Xian-Zhu Fu, Gui-Hua Zhou, Jing-Li Luo, Karl T. Chuang, and Alan R. Sanger

Department of Chemical and Materials Engineering, University of Alberta, Edmonton, AB, Canada T6G 2G6

Correspondence should be addressed to Jing-Li Luo, jingli.luo@ualberta.ca

Received 15 May 2011; Accepted 22 July 2011

Academic Editor: Milan M. Jaksic

Ethylene and electrical power are cogenerated in fuel cell reactors with $FeCr_2O_4$ nanoparticles as anode catalyst, $La_{0.7}Sr_{0.3}FeO_{3-\delta}$ (LSF) as cathode material, and $BaCe_{0.7}Zr_{0.1}Y_{0.2}O_{3-\delta}$ (BCZY) perovskite oxide as proton-conducting ceramic electrolyte. $FeCr_2O_4$, BCZY and LSF are synthesized by a sol-gel combustion method. The power density increases from 70 to 240 mW cm^{-2}, and the ethylene yield increases from about 14.1% to 39.7% when the operating temperature of the proton-conducting fuel cell reactor increases from 650°C to 750°C. The $FeCr_2O_4$ anode catalyst exhibits better catalytic performance than nanosized Cr_2O_3 anode catalyst.

1. Introduction

Solid oxide fuel cells (SOFC) are promising as clean power sources having high energy conversion efficiency and excellent fuel flexibility. Typically, SOFC are based on an oxygen-ion-conducting electrolyte, which usually requires high operating temperature. In the last few years, an ever-growing interest has been directed toward proton-conducting electrolytes for intermediate or low-temperature SOFC applications [1]. Among these, the most investigated proton-conducting electrolytes are doped perovskite oxides (ABO_3), in which the A sites are occupied by alkaline earth elements such as Ba, Sr, and Ca, and B sites are occupied by tetravalent elements (usually Ce or Zr), and these perovskites are doped with trivalent ions such as Y, Nd, Sm, Yb, and In to increase the density of oxide ion vacancies required for ion conductivity. Among these electrolytes Y-doped barium cerate (BCY) stands out for its high proton conductivity but it has insufficiently high chemical stability as, for example, it reacts readily with CO_2 or SO_2. On the other hand, Y-doped barium zirconate (BZY) shows good chemical stability but suffers from insufficient proton conductivity. When codoped with Y and Zr, barium cerate (BCZY) has balanced conductivity and chemical stability in reactive environments [2, 3].

Ethylene is an important feedstock in the petrochemical industry, and its demand is expected to increase significantly in the near future [4, 5]. Currently, ethylene is produced mainly by steam cracking of naphtha or ethane, FCC (fluid catalytic cracking), and catalytic dehydrogenation of ethane. However, when steam cracking is operated at high temperature the process consumes much energy and has a low selectivity to ethylene and unavoidable coke formation. Recently, ethane-fueled proton-conducting ceramic fuel cell reactors have been developed to cogenerate ethylene and electrical energy with high efficiency [6–11]. This reaction system has several specific advantages including high selectivity to ethylene and low impact on the environment, as there are very little or no greenhouse gas (CO_2) emissions. In a proton-conducting fuel cell reactor, the dehydrogenation of ethane to ethylene and hydrogen (forming protons) is conducted over the anode catalyst, while the protons are conducted through the proton conducting electrolyte to the cathode side and reacted with oxygen to form water. Electrons are conducted through an external circuit during this reaction.

Catalysts are needed to achieve more efficient power production and utilization of ethane resources and higher activity and selectivity to ethylene of reaction at the anode. Recently, nanosized Cr_2O_3 particles prepared by a sol-gel combustion method were proven to be effective and stable anode catalysts for the process [6]. Such metal oxides, especially in the form of solid solutions, are interesting solids due to their surface acid-base properties and oxidation-reduction potentials. Chromium iron oxide catalysts, in particular, have been explored for the last two decades for their superior catalytic activity in processes such as the water-gas-shift (WGS) reaction [12, 13], conversion of methanol [14], Fischer Tropsch synthesis [15], when compared with the corresponding Fe- or Cr-alone catalysts. Now precipitated Fe,Cr-containing oxide catalysts are used commercially for the high-temperature WGS reaction.

In previous studies Pt often was used as both anode and cathode catalysts. However, Pt is expensive and easily poisoned by carbon deposition at fuel cell operating temperature. Herein, we report the fabricating and testing of electrolyte-supported fuel cells using chromium iron oxide nanoparticles ($FeCr_2O_4$) as anode catalyst, $La_{0.7}Sr_{0.3}FeO_{3-\delta}$ as cathode material, and $BaCe_{0.7}Zr_{0.1}Y_{0.2}O_{3-\delta}$ as electrolyte for coproduction of ethylene and electrical power. The catalytic performance, electrical performance, and resistance of the fuel cell also are described.

2. Experimental

2.1. Materials Preparation and Characterization. $FeCr_2O_4$ nanopowders were prepared using a sol-gel method [16, 17]. $Cr(NO_3)_3 \cdot 6H_2O$, and $Fe(NO_3)_3 \cdot 6H_2O$ were first dissolved in deionized water. Subsequently, citric acid as chelating agent was added in 2 : 1 molar ratio to metal ions. The resulting solution was adjusted to about pH 8 with ammonium hydroxide, then heated on a hot plate to evaporate water at 90°C until it formed a gel which then was dried. The dry gel was calcined at 500°C for 4 h.

$BaCe_{0.7}Zr_{0.1}Y_{0.2}O_{3-\delta}$ (BCZY) perovskite nanopowders were prepared using a citric acid-nitrate combustion method. $Ba(NO_3)_2$, $Ce(NO_3)_3 \cdot 6H_2O$, $ZrO(NO_3)_2 \cdot 2.6H_2O$, and $Y(NO_3)_3 \cdot 6H_2O$ were first dissolved in deionized water. Subsequently, citric acid as chelating agent and NH_4NO_3 as oxidant agent were added in molar ratio of citric acid: total metal ions: NH_4NO_3 of 1.5 : 1 : 3. The resulting solution was adjusted to about pH 8 with ammonium hydroxide and heated on a hot plate to evaporate water until it changed into brown foam and then ignited. After combustion, the obtained ash was calcined at 1000°C in air for 6 h to obtain BCZY powders.

The $La_{0.7}Sr_{0.3}FeO_{3-\delta}$ (LSF) perovskite nanopowders were synthesized using the same method used for BCZY, described above. $La(NO_3)_3 \cdot 6H_2O$, $Sr(NO_3)_2 \cdot 6H_2O$, and $Fe(NO_3)_3 \cdot 9H_2O$ were the reactants. The obtained ash was calcined at 800°C in air for 5 h to obtain LSF powders.

The phase structures of materials were identified using a Rigaku Rotaflex X-ray diffractometer (XRD) with Co Kα radiation. The morphology of sintered BCZY disc cross sections was determined using a Hitachi S-2700 scanning electron microscope (SEM).

2.2. Fuel Cell Reactor Fabrication. Dense BCZY electrolyte pellets were fabricated via a pressing method. The nanosized powder was first pressed at 5 tonnes in a stainless-steel die with 1.86 cm ID to form a substrate disc, which was sintered at 1500°C for 10 h to obtain a nonporous, dense BCZY thick film. An intimate mixture comprising similar weights of $FeCr_2O_4$, Cu powder, and BCZY was dispersed in terpineol mixed with 10% polyethylene glycol (PEG) as screen printing binder to form a paste. This paste was screen painted onto one side of the electrolyte and dried under infrared light to form the anode. A mixture of 50% LSF and 50% BCZY was pasted onto the opposite side to form the cathode. The cell then was heated at 950°C for 4 h in air to achieve strong bonding between the electrolyte and electrode materials.

2.3. Fuel Cell Reactor System Fabrication and Test. The fuel cell reactor setup and the testing system were as described previously [6]. The fuel cell reactor was set up by securing the MEA (membrane electrode assembly) between coaxial pairs of alumina tubes and sealed using ceramic sealant, which was cured by heating in a vertical Thermolyne F79300 tubular furnace. Au paste and mesh were used to make the current collector at both electrodes. 10% H_2 (balance with He) was fed into the anode chamber as the temperature was increased from room temperature to 750°C at 1°C/min. Then, ethane was fed into the anode chamber to replace the 10% H_2 feed. The cathode feed was oxygen.

The electrochemical performance of fuel cell reactors was measured using a Solartron 1287 electrochemical interface together with 1255B frequency response analysis instrumentation. The outlet gases from the anode chamber were analyzed using a Hewlett-Packard model HP5890 GC equipped with a packed bed column (OD: 1/8″; length: 2 m; packing: Porapak QS) operated at 80°C and equipped with a thermal conductivity detector. The ethane conversion and ethylene selectivity were calculated according to the previously reported method [9].

3. Results and Discussion

3.1. Textural and Structural Properties. The phases of the electrode and electrolyte materials were determined using X-ray diffraction (XRD). Figure 1(a) shows the XRD patterns of the $La_{0.7}Sr_{0.3}FeO_{3-\delta}$ cathode and the $BaCe_{0.7}Zr_{0.1}Y_{0.2}O_{3-\delta}$ electrolyte after firing. It can be seen that all samples were a single perovskite phase, without detectable amounts of any impurities. Figure 1(b) compares the XRD spectra of fresh and reduced Fe,Cr-based anode catalyst. XRD confirmed that pure $FeCr_2O_4$ phase (JCPDS Card No. 34-0140) was formed after calcination of the Fe,Cr-citrate complex gel at 500°C for 4 h in air. When this material was reduced in H_2 at 750°C for 4 h, some iron ions were reduced to metallic iron nanoparticles. However, the remaining ions remained present as the $FeCr_2O_4$ phase.

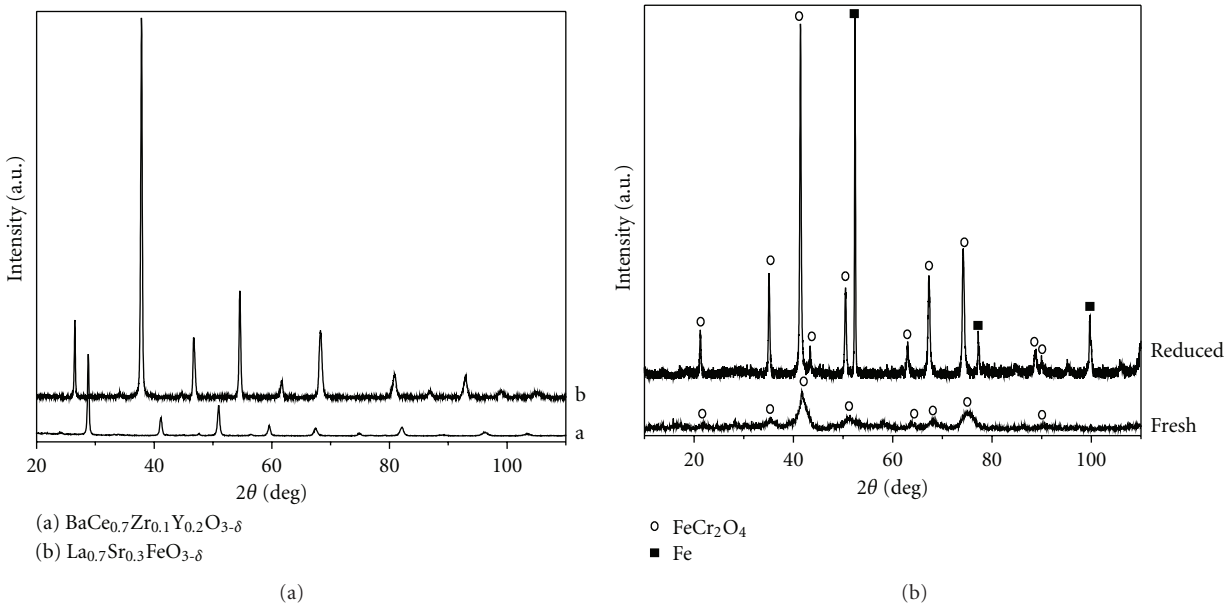

Figure 1: XRD patterns for: (a) $La_{0.7}Sr_{0.3}FeO_{3-\delta}$ and $BaCe_{0.7}Zr_{0.1}Y_{0.2}O_{3-\delta}$, and (b) $FeCr_2O_4$ catalysts before and after being reduced by H_2.

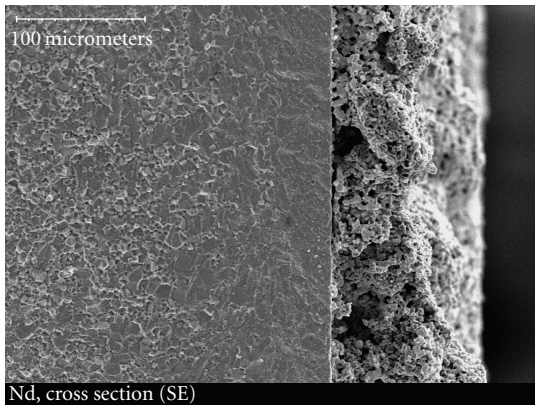

Figure 2: SEM image of a cross section of the BCZY electrolyte-supported cell with $FeCr_2O_4$ catalyst.

The XRD peaks of fresh $FeCr_2O_4$ phase were broadened due to the small crystalline size. From the line broadening of the diffraction peak at 42°, the average crystallite sizes of the catalysts were calculated using the Scherrer Formula ($T = 0.89\lambda/\beta\cos\theta$). The fresh catalyst crystallites averaged only 4.2 nm. Thus, using citrate as a chelating agent provided good distribution of Fe and Cr ions throughout the dry gel, generated a large amount of gas during the citrate-nitrate gel combustion and decomposition, and so the combination of these effects resulted in the formation of very fine particles. When the catalysts were reduced in H_2 at high temperature of 750°C for 4 h, the crystallite size increased to 33.6 nm.

Figure 2 shows a typical scanning electron microscopy (SEM) image of the electrolyte supported fuel cell. The BCZY electrolyte was dense, thus it separates the anode and cathode feeds very well. The image also shows the typical porous microstructure of the electrodes, required to achieve good diffusion of feed to the electrochemically active triple phase boundary sites (TPB).

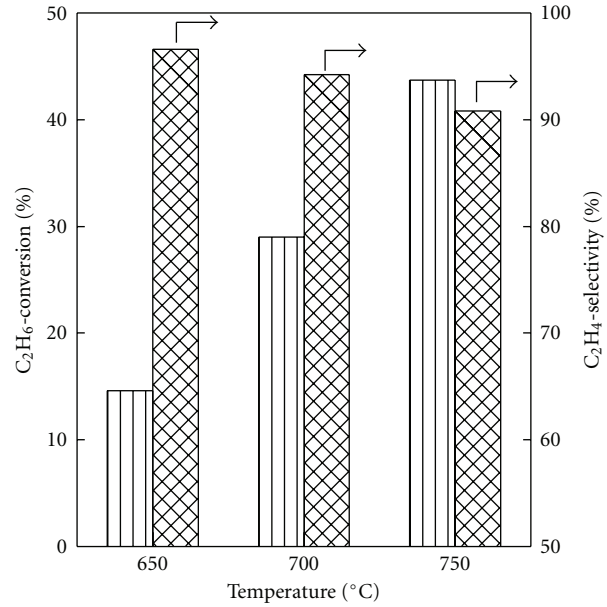

Figure 3: Ethane conversion and ethylene selectivity for a $FeCr_2O_4$-BCZY|BCZY|LSF-BCZY single cell as a function of temperature. The flow rates of ethane and oxygen are each 150 mL/min.

3.2. Catalytic Performance. At elevated temperatures the main reaction in the anode chamber was dehydrogenation of ethane to ethylene with high selectivity, with cogeneration of electricity. Figure 3 shows the ethane conversion and ethylene selectivity at different reaction temperatures. The conversion of ethane increased from 14.6% to 29% and 43.7% whilst

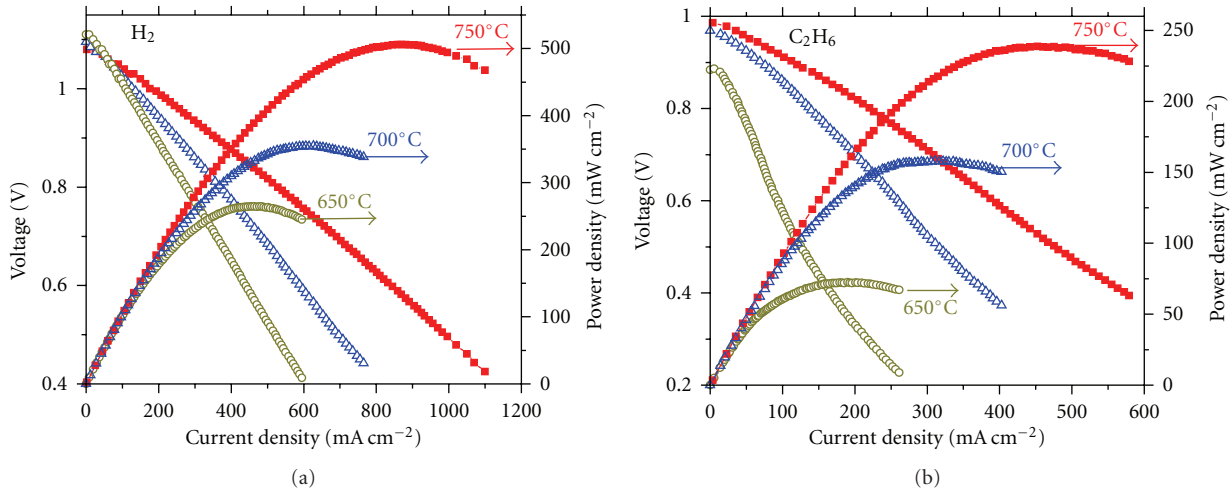

Figure 4: I–V curves and power density output of the $FeCr_2O_4$-BCZY|BCZY|LSF-BCZY single cell at different temperatures with (a) hydrogen and (b) ethane as the fuel.

the selectivity to ethylene decreased from 96.6% to 94.2% and 90.8% as the operating temperature increased from 650°C to 700°C and then 750°C. The ethane conversions over this nanosized $FeCr_2O_4$ catalyst were higher than the values over Cr_2O_3 catalysts under the same conditions, described in our previous study [6]. In that study, conversion of ethane increased from 8.5% to 35.3% whilst the selectivity of ethylene decreased from 98.6% to 88.2% as the operating temperature increased from 650 to 750°C. Cr_2O_3 is widely used as an excellent dehydrogenation catalyst, and so dehydrogenation of ethane to ethylene occurred readily [18]. However, the present $FeCr_2O_4$ catalyst showed even better catalytic performance than Cr_2O_3 nanoparticles.

The differences between GC analyses of the anode feed and effluent showed the formation of small but increasing amounts of methane and hydrogen and traces of carbon oxides, as the rate of dehydrogenation of ethane increased with temperature. The hydrogen in the anode outlet was attributable to either or both of the gas phase cracking of ethane and the more rapid catalytic production of H_2 than could be accommodated by conduction of protons through the thick electrolyte membrane used in this study. Methane was produced from the thermal cracking of ethane which, as expected, was more favoured at the higher temperature, so that ethylene selectivity decreased while methane selectivity increased with temperature. The amounts of CO_2 formed were traces. The proton-conducting ceramic electrolyte membrane prevented contact with any oxygen source other than the oxide materials themselves and the very small amount of oxide conductivity in the electrolyte, as the proton ceramic electrolyte membrane conducted the protons to the cathode to react with oxygen and form water, thus providing the thermodynamic driving force and removing equilibrium limitation of the dehydration reaction.

3.3. Electrochemical Performance. To investigate the electrochemical performance of the $FeCr_2O_4$ anode under fuel cell operating conditions a single cell based on BCZY electrolyte was tested in the range from 650°C to 750°C using different types of fuel. Figure 4 shows the I–V and power density curves (after manual compensation) of the single cell using pure hydrogen (Figure 4(a)) or ethane (Figure 4(b)) as fuel. The open-circuit voltages (OCVs) of 1.04, 1.07, and 1.1 V for H_2 fuel and 0.98, 0.95, and 0.88 V for C_2H_6 fuel at 750, 700, and 650°C, respectively, indicated that the BCZY electrolyte was dense and impermeable. The OCV value decreased as the temperature increased for the tests with H_2 as fuel. In contrast, the trend was the inverse when C_2H_6 was used as fuel. The OCV for C_2H_6 fuel was lower than that when using H_2 as fuel. These trends suggest that the dissolution rate of a proton generated from C_2H_6 fuel into the electrolyte bulk was slower than that of a proton generated from H_2 as fuel, probably as a consequence of the relative rates of generation of protons from the respective feeds. The maximum power densities were 510, 360, and 250 mW cm^{-2} for H_2 fuel and 240, 160, and 70 mW/cm^{-2} for C_2H_6 fuel at 750, 700, and 650°C, respectively. The high power density values indicated that the $FeCr_2O_4$ material is a suitable candidate as an anode catalyst for proton-conducting SOFC. The high performance of the cell is attributable mainly to the high activity of H_2 on the $FeCr_2O_4$ surface and the Fe metallic sites. Comparison of these power density values suggested that the $FeCr_2O_4$-based anode had higher catalytic activity for the electrochemical oxidation of H_2 than for that of C_2H_6.

In order to further compare the different contributions to the total resistance with H_2 or C_2H_6 as fuel in the single cell test, electrochemical impedance spectroscopy measurements were performed under open-circuit conditions at different temperatures, as shown in Figure 5. The intercept with the real axis at high frequency represented the ohmic resistance (R_{ohm}) of the cell which, reasonably, was usually taken as the overall electrolyte resistance of the cell. The difference between the high-frequency and low-frequency intercepts with the real axis represented the total interfacial polarization resistance (R_p) of the cell. The overall electrolyte

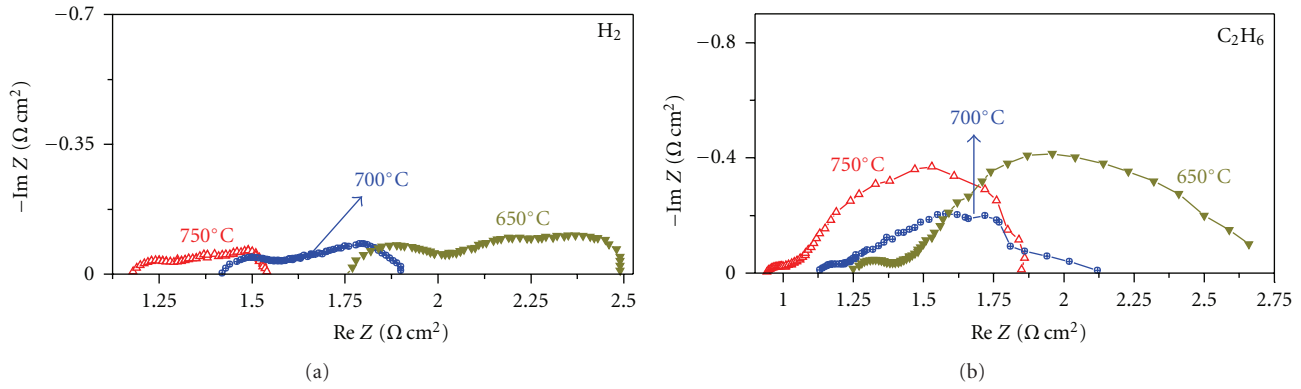

FIGURE 5: Electrochemical impedance spectra of the $FeCr_2O_4$-BCZY|BCZY|LSF-BCZY single cell at different temperatures, with (a) hydrogen and (b) ethane as the fuel.

resistances of the cell were 1.19, 1.42, and 1.75 $\Omega\,cm^2$ for H_2 fuel and 0.94, 1.12, and 1.24 $\Omega\,cm^2$ for C_2H_6 fuel at 750, 700, and 650°C, respectively. The corresponding polarization resistances (R_E) of the cell were 0.35, 0.48, and 0.78 $\Omega\,cm^2$ for H_2 fuel and 0.91, 1.02 and 1.44 $\Omega\,cm^2$ for C_2H_6 fuel. Apparently, as the operating temperature was decreased, R_{ohm} and R_p, the two specific contributions to the total resistance, both increased dramatically. R_{ohm} was predominant for the test using H_2 as fuel, while R_{ohm} and R_p had comparable values for the tests using C_2H_6 as fuel. The impedance arcs for both the H_2 fuel and C_2H_6 fuel decreased significantly with the increase in temperature. It is interesting that the impedance responses of the ethane fuel tests became clearly separated at high frequencies. This indicated that the H_2 oxidation reaction on $FeCr_2O_4$ anodes was controlled by at least two distinct electrode processes. In addition, it is obvious that the R_{ohm} in C_2H_6 fuel is a little lower than that in H_2 fuel. A similar phenomenon was observed for the Cu-Ce-YSZ fuel cell fed by hydrogen and *n*-butane [19]. It has been reported that the value of R_{ohm} of Cu-Ni alloy cermets decreased with time after long-time exposure to methane [20]. It was suggested that deposition of hydrocarbons in the anode improves the connectivity between catalyst particles and decreases the ohmic resistance [19, 20].

In each of the fuel cell tests the activation polarization was very similar in value, which meant that the activation ability of $FeCr_2O_4$ catalysts for H_2 and C_2H_6 varied little with temperature. Overall, the plots (Figure 5) each consisted of a small higher-frequency depressed arc and a large lower-frequency arc, the sizes of both of which increased with decreasing temperature, as typically observed for electrochemical processes such as charge transfer or surface diffusion. However, in each case the arcs were envelopes of a series of overlapping arcs. The overlapping arcs may arise from the presence of both nano-Fe particles and $FeCr_2O_4$ in the anode catalyst (Figure 1). While it is not possible to unequivocally determine this from the present data and further investigation is required, it is known that Fe particles are active catalysts for alkane dehydrogenation, including isobutane to isobutene [21].

The high values of the ohmic resistance were attributable to the overall configuration of the single cell, in particular the large thickness of the BCZY electrolyte (about 0.9 mm), suggesting that higher performance should be attainable from cells with much thinner electrolyte layers.

4. Conclusions

An electrolyte-supported proton-conducting SOFC fabricated using $FeCr_2O_4$ as the anode catalyst, and LSF as the cathode has high performance for conversion of ethane to cogenerate ethylene and electrical power. The fuel cell reactor provides high selectivity, over 90%, for ethane dehydrogenation and ethylene yields of 14.1, 27.3 and 39.7%, while cogenerating 70, 160, and 240 mW cm^{-2} power densities at 650, 700, and 750°C, respectively. The ethane conversions over this nanosized $FeCr_2O_4$ catalyst are notably higher than the values over previously described Cr_2O_3 catalysts.

Acknowledgments

This work was supported by the Natural Sciences and Engineering Research Council of Canada/NOVA Chemicals CRD Grant, the Alberta Energy Research Institute, and the Micro Systems Technology Research Institute. The authors thank Dr. Juri Melnik for very helpful discussions.

References

[1] E. Fabbri, D. Pergolesi, and E. Traversa, "Electrode materials: a challenge for the exploitation of protonic solid oxide fuel cells," *Science and Technology of Advanced Materials*, vol. 11, no. 4, article 044301, 2010.

[2] K. Katahira, Y. Kohchi, T. Shimura, and H. Iwahara, "Protonic conduction in Zr-substituted $BaCeO_3$," *Solid State Ionics*, vol. 138, no. 1-2, pp. 91–98, 2000.

[3] Y. Guo, Y. Lin, R. Ran, and Z. Shao, "Zirconium doping effect on the performance of proton-conducting $BaZr_yCe_{0.8-y}Y_{0.2}O_{3-\delta}$ ($0.0 \le y \le 0.8$) for fuel cell applications," *Journal of Power Sources*, vol. 193, no. 2, pp. 400–407, 2009.

[4] F. Cavani, N. Ballarini, and A. Cericola, "Oxidative dehydrogenation of ethane and propane: how far from commercial implementation?" *Catalysis Today*, vol. 127, no. 1–4, pp. 113–131, 2007.

[5] D. Akporiaye, S. F. Jensen, U. Olsbye et al., "A novel, highly efficient catalyst for propane dehydrogenation," *Industrial and Engineering Chemistry Research*, vol. 40, no. 22, pp. 4741–4748, 2001.

[6] X. Z. Fu, X. X. Luo, J. L. Luo, K. T. Chuang, A. R. Sanger, and A. Krzywicki, "Ethane dehydrogenation over nano-Cr_2O_3 anode catalyst in proton ceramic fuel cell reactors to co-produce ethylene and electricity," *Journal of Power Sources*, vol. 196, no. 3, pp. 1036–1041, 2011.

[7] C. K. Cheng, J. L. Luo, K. T. Chuang, and A. R. Sanger, "Propane fuel cells using phosphoric-acid-doped polybenzimidazole membranes," *Journal of Physical Chemistry B*, vol. 109, no. 26, pp. 13036–13042, 2005.

[8] W. S. Li, D. S. Lu, J. L. Luo, and K. T. Chuang, "Chemicals and energy co-generation from direct hydrocarbons/oxygen proton exchange membrane fuel cell," *Journal of Power Sources*, vol. 145, no. 2, pp. 376–382, 2005.

[9] S. Wang, J. L. Luo, A. R. Sanger, and K. T. Chuang, "Performance of ethane/oxygen fuel cells using yttrium-doped barium cerate as electrolyte at intermediate temperatures," *Journal of Physical Chemistry C*, vol. 111, no. 13, pp. 5069–5074, 2007.

[10] Z. Shi, J. L. Luo, S. Wang, A. R. Sanger, and K. T. Chuang, "Protonic membrane for fuel cell for co-generation of power and ethylene," *Journal of Power Sources*, vol. 176, no. 1, pp. 122–127, 2008.

[11] X. Z. Fu, J. L. Luo, A. R. Sanger, Z. R. Xu, and K. T. Chuang, "Fabrication of bi-layered proton conducting membrane for hydrocarbon solid oxide fuel cell reactors," *Electrochimica Acta*, vol. 55, no. 3, pp. 1145–1149, 2009.

[12] Y. Lei, N. W. Cant, and D. L. Trimm, "Kinetics of the water-gas shift reaction over a rhodium-promoted iron-chromium oxide catalyst," *Chemical Engineering Journal*, vol. 114, no. 1–3, pp. 81–85, 2005.

[13] BASF, vol. German Offen 254572, 1911.

[14] A. Khaleel, I. Shehadi, and M. Al-Shamisi, "Nanostructured chromium-iron mixed oxides: physicochemical properties and catalytic activity," *Colloids and Surfaces A*, vol. 355, no. 1–3, pp. 75–82, 2010.

[15] A. A. Khassin, A. G. Sipatrov, M. P. Demeshkina, and T. P. Minyukova, "Partially hydrated iron-chromium oxide catalyst for the Fischer-Tropsch synthesis," *Reaction Kinetics and Catalysis Letters*, vol. 97, no. 2, pp. 371–379, 2009.

[16] J. Livage, "Sol-gel processes," *Current Opinion in Solid State and Materials Science*, vol. 2, no. 2, pp. 132–138, 1997.

[17] J. D. Mackenzie and E. P. Bescher, "Chemical routes in the synthesis of nanomaterials using the sol-gel process," *Accounts of Chemical Research*, vol. 40, no. 9, pp. 810–818, 2007.

[18] B. M. Weckhuysen and R. A. Schoonheydt, "Alkane dehydrogenation over supported chromium oxide catalysts," *Catalysis Today*, vol. 51, no. 2, pp. 223–232, 1999.

[19] S. McIntosh, J. M. Vohs, and R. J. Gorte, "Role of hydrocarbon deposits in the enhanced performance of direct-oxidation SOFCs," *Journal of the Electrochemical Society*, vol. 150, no. 4, pp. A470–A476, 2003.

[20] H. Kim, C. Lu, W. L. Worrell, J. M. Vohs, and R. J. Gorte, "Cu-Ni cermet anodes for direct oxidation of methane in solid-oxide fuel cells," *Journal of the Electrochemical Society*, vol. 149, no. 3, pp. A247–A250, 2002.

[21] H. Shimada, T. Akazawa, N. O. Ikenaga, and T. Suzuki, "Dehydrogenation of isobutane to isobutene with iron-loaded activated carbon catalyst," *Applied Catalysis A*, vol. 168, no. 2, pp. 243–250, 1998.